Met Office

Improved parametrization scheme to represent tropospheric moist convection in the atmospheric dispersion model NAME

Forecasting Research Technical Report No: 639

31/12/2019

E. Meneguz[1], M. Filus[2], V. Selvaratnam[1], D. J. Thomson[1], N. R. P. Harris[3], C. S. Witham[1], M. A. Navarro[4†] and E. L. Atlas[4]

[1]Met Office

[2]Dept. of Chemistry, University of Cambridge

[3]Centre for Environmental and Agricultural Informatics, Cranfield University

[4]Dept. of Atmospheric Sciences, RSMAS, University of Miami

[†]Deceased 19th December 2017

Abstract

This paper describes the development of a scheme to parametrize tropospheric convection in the Met Office's Numerical Atmospheric-dispersion Modelling Environment (NAME). A Lagrangian dispersion model, NAME is generally driven by meteorological data from an NWP model. The new convection scheme is intended to represent particle transport due to the presence of precipitating convective clouds whose horizontal scale is not captured by the NWP model resolution. The scheme can be used both in forward and backward time mode and is based on the balance equations for the convective mass, entrainment and detrainment fluxes. Such fluxes are used to estimate how many particles entrain, move upward/downward and detrain. To investigate the performance of NAME with and without the parametrization of convection, two case studies are set up over the Tropical West Pacific Warm Pool, known to be one of the most convective regions on the globe. It is shown that the implementation of the new scheme leads to a more realistic estimate of particle vertical transport in the troposphere. NAME modelled mixing ratios of methyl iodide (CH_3I) are compared with values measured at altitudes between 14 to 18 km asl during four flights from the NASA ATTREX campaign. It is found that simulations with the new parametrization scheme significantly decrease the gap between modelled and observational data, improving the overall performance of the NAME model.

1 Introduction

Atmospheric convection plays a large part in transport and mixing above the boundary layer and results in a large exchange of heat and energy [10]. In moist convection, updraughts and downdraughts occurring inside convective clouds play a key role in redistributing gases and aerosols through the troposphere. Although the intensity of moist atmospheric convection is particularly high over the tropical regions, convective cells originate nearly everywhere on the globe including at mid-latitudes and can be important in long range transport of pollutants.

The second half of the twentieth century saw the birth and development of atmospheric dispersion models in the international scientific community. Such models are now used to forecast the transport of a wide range of airborne pollutants such as radioactive, chemical and volcanic substances, odours, airborne animal viruses, as well as to provide routine air quality forecasts. In the case of emergency response, both model accuracy and time efficiency is crucial to deliver real-time information to government bodies. Among the modelling approaches used is the *Lagrangian* particle technique which represent pollutants as model particles that are transported by the resolved wind field and by random velocities generated by a stochastic process to represent unresolved processes. The resolved wind field is generally provided by a Numerical Weather Prediction (NWP) model. This is the approach used by FLEXPART [31], STILT [22], the Canadian Meteorological Centre's Atmospheric Transport and Dispersion Modelling Suite [8], HYSPLIT [30], NAME [21] and TAPM [19], although in some of these models it can be supplemented by other approaches.

For long range dispersion models, the horizontal scale on which convection exists is usually

below the horizontal resolution of the NWP model used. This can be addressed by introducing parametrizations to represent the vertical motions undertaken by pollutants due to the presence of precipitating convective clouds, which would otherwise be under-represented.

The subject of this paper is a convective parametrization scheme developed in the Numerical Atmospheric-dispersion Modelling Environment (NAME) and its testing and validation. The article is structured as follows. In section 2, a brief description of the working principles of NAME with particular emphasis on long range transport is followed by a detailed explanation of the new scheme for convective parametrization. In section 3, the performance of the scheme is evaluated in terms of backward-forward probability equivalence, and consideration is given to the fulfillment of the well-mixed condition. The object of section 4 is the illustration and discussion of two case studies used to evaluate the difference between NAME simulations with and without the new parametrization of convection (case study I) and to benchmark NAME modelled mixing ratios of methyl iodide to observations (case study II). Lastly, concluding remarks and suggestions for future improvements are given in section 5.

2 Convective parametrization scheme in NAME for long-range transport of pollutants

2.1 Working principles of NAME

NAME is the Lagrangian particle model developed by the Met Office (UK) following the Chernobyl power-plant accident in 1986 to provide detailed predictions of the transport and deposit of radioactive material. Since then, the model has undergone significant further development [21] and is currently used to advise the British government and regulatory bodies for emergency response and operational forecasts, as well as for research activities on a wide range of atmospheric dispersion events (nuclear and chemical accidents, volcanic eruptions and smoke from fires to mention but a few).

Emissions into the atmosphere from a pollutant source (either of gaseous or particulate matter) are simulated by releasing a large number of model particles, each representing a certain proportion of the mass or activity of released pollutants. Following a Lagrangian approach, the particles are then tracked individually along the flow and advected by the three-dimensional wind field (supplied through the input meteorology) with turbulent dispersion processes and unresolved mesoscale eddies parametrized using Monte Carlo techniques ([14]). The meteorology is interpolated in time and space to the particle's position. For long-range simulations, stochastic differentential equations which correspond to diffusion processes for the particle position are used to represent the turbulence and unresolved mesoscale eddies, while, for short-range simulations, a more sophisticated option is available where the stochastic differential equations are formulated in position-velocity space. Model particles can also evolve with time to account for various atmospheric processes that

might transform or remove the pollutants (e.g. radioactive decay, chemical transformations, and dry/wet deposition).

NAME can be used with multiple sources of NWP data and other flow information on a 3-dimensional gridded domain, which is then interpolated to the particle position. Although usually NAME relies on the Met Office's operational weather prediction model data, the Unified Model (UM) [7], in principle it can handle most other meteorological input datasets (such as WRF and ECMWF data). When coupled with high resolution meteorological data obtained from an NWP model with convection permitting dynamics (such as the current 1.5 km resolution UK model) it is assumed that convective cloud and precipitation are resolved. Consequently, in this case no additional convective parametrization scheme is used in NAME. However with coarser resolution meteorological data that does not resolve convection (such as the Met Office's current global model) a convective parametrization is required. The convective parametrization scheme described in the remainder of this section has recently been added in NAME to simulate displacement of particles due to moist convection taking place in the troposphere. It does not treat mixing within the convective boundary layer which is represented as part of the turbulence parametrization scheme ([23]; [34]). This scheme replaces a much simpler older scheme [23] in which, whenever the convective cloud depth exceeded a critical value, a number of particles proportional to the cloud fraction were randomly redistributed between the cloud base and top.

2.2 New scheme for parametrization of moist tropospheric convection

While our approach owes much to [13] and, in particular, to [6], our intention was produce a scheme which can be run using the diagnostic fields readily available from NWP models such as the UM, avoiding the need to obtain detailed diagnostics from the NWP convection parametrization (as required by [6]), while also avoiding the need to run a full NWP convection parametrization within NAME itself (as in the approach of [13]). The potential for possible future tighter coupling between NAME and the UM, with access to more detailed diagnostics from the UM, has also been a guiding criterion while designing the scheme. The preliminary stages of the development of the scheme were described in [24] but this paper illustrates the full development of the scheme, including the capability to be run backwards in time. An 'operatior splitting' approach is used, with the convective evolution over the time step Δt calculated in a separate step which occurs after the advection due to (i) the resolved flow, (ii) the unresolved mesoscale eddies, and (iii) the turbulence.

2.2.1 Cloud pressure grid

Deep convective clouds are represented in NAME as a series of layers (see Figure 1), with base and top determined by the NWP-diagnosed convective cloud base and convective cloud top respectively. If the NWP model has convection over more than one vertical region at a given horizontal position, only the lowest region of convection is currently considered.

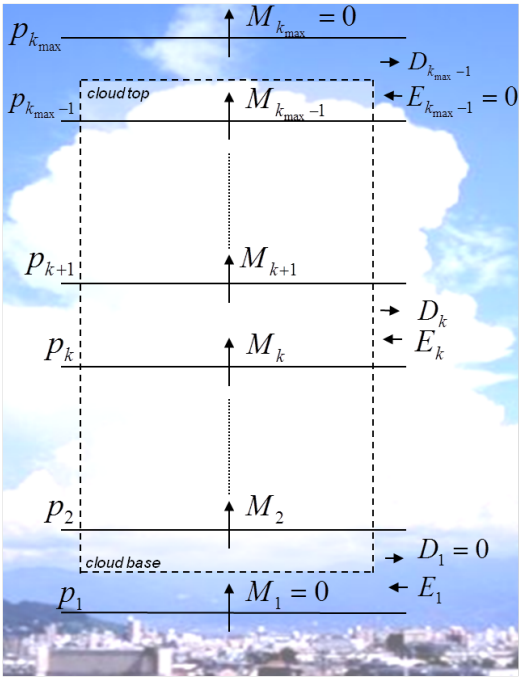

Figure 1: Simplified representation of a convective cloud as a rectangular shape (dashed lines) with exchange of air from/to the environment according to the mass-flux approach (in forward mode). Solid horizontal lines correspond to pressure levels, horizontal arrows to the entrainment and detrainment fluxes and vertical arrows to the updraught mass fluxes.

To conveniently represent the transport of air inside the cloud, from the cloud to the environment (detrainment) and from the environment to the cloud (entrainment), pressure is chosen as a suitable coordinate and an *ad hoc* vertical grid of equally spaced pressure levels is built. The total number of pressure levels, k_{max}, is chosen depending on the vertical extent of the cloud, but a minimum of 3 and a maximum of 51 is imposed, with the minimum chosen to guarantee that there is at least one pressure level below the cloud base, one inside the cloud and one above the cloud. The pressure levels p_k, $k \in [1, k_{max}]$, and level spacing or layer thickness Δp are then chosen so that the cloud base and top are, in terms of pressure, in the middle of the bottom and top layers (unless this puts p_1 below ground when we ensure that p_1 equals the surface pressure p_0 and that the cloud top is in the middle of the top layer).

2.2.2 The mass-flux approach

The parametrization scheme developed in the UM uses mass fluxes to represent atmospheric convection. Convective updraughts and downdraughts are modelled. It is based on [15] but has since undergone significant development; for example, from around 2005 the adaptive detrainment option [9] became standard. The convection parametrization in NAME also uses mass fluxes, but is simpler both in the way the mass fluxes are determined and in (currently) including only updraughts.

The equation of conservation of mass can be written, in discretized form, as:

$$M_{k+1} + D_k = M_k + E_k \tag{1}$$

where M_k is the updraught mass flux at pressure level k and E_k and D_k are respectively the entrainment and detrainment mass fluxes in the layer between p_k and p_{k+1} (see Figure 1). The mass fluxes are defined in units of Pa/s, this choice of unit being consistent with that adopted in the UM convection scheme (and corresponding strictly to a 'weight flux'). In not including downdraughts, the parametrization scheme is similar to that of [6] although different from the approach of [13]. The neglect of downdraughts is a reasonable approximation because downdraught mass fluxes are generally much smaller than updraught fluxes (typically around one tenth as big). However, including downdraughts would be a useful future extension of the model.

The mass fluxes from the UM convection scheme are not available yet for operational use in NAME and their representation is therefore challenging. The next subsection illustrates how they are estimated in the new convection scheme.

2.2.3 Updraught mass flux profile shapes

Non-dimensional updraught mass flux profiles are obtained using empirical formulas (Grant, A.L.M, December 2012, pers. comm.) derived from Cloud Resolving Models. These formulas are based on the pressure of the freezing level p_{fl}, the cloud top p_{ct}, the cloud base p_{cb} and a reference minimum pressure difference p_{min} which is taken to be 100 hPa. If $p_{fl} - p_{ct} \geq p_{min}$ and $p_{cb} - p_{fl} \geq p_{min}$, then the updraught mass flux at pressure level k, non-dimensionalised with the cloud base mass flux, is given by:

$$\hat{M}_k = \begin{cases} \hat{M}_{max} \exp\left(-\beta_1 \left(\dfrac{p_k - p_{fl}}{p_{cb} - p_{fl}}\right)^2\right) & \text{if } p_k \geq p_{fl} \\ \hat{M}_{max} \exp\left(-\beta_2 \left(\dfrac{p_k - p_{fl}}{p_{ct} - p_{fl}}\right)^2\right) & \text{if } p_k < p_{fl} \end{cases} \tag{2}$$

and the mass flux profile has a maximum at the freezing level. This is intended to represent the updraught mass flux profile in the tropics. Otherwise:

$$\hat{M}_k = \hat{M}_{max} \exp\left(-\beta_2 \left(\frac{p_k - p_{cb}}{p_{ct} - p_{cb}}\right)^2\right) \tag{3}$$

i.e. the mass flux profile decreases with height in warm rain clouds (with tops below the freezing level) and in cold air clouds (with base above the freezing level). While this might not be intuitive, it is supported by experimental and numerical evidence (see e.g. [35] for the warm rain case). In (2)

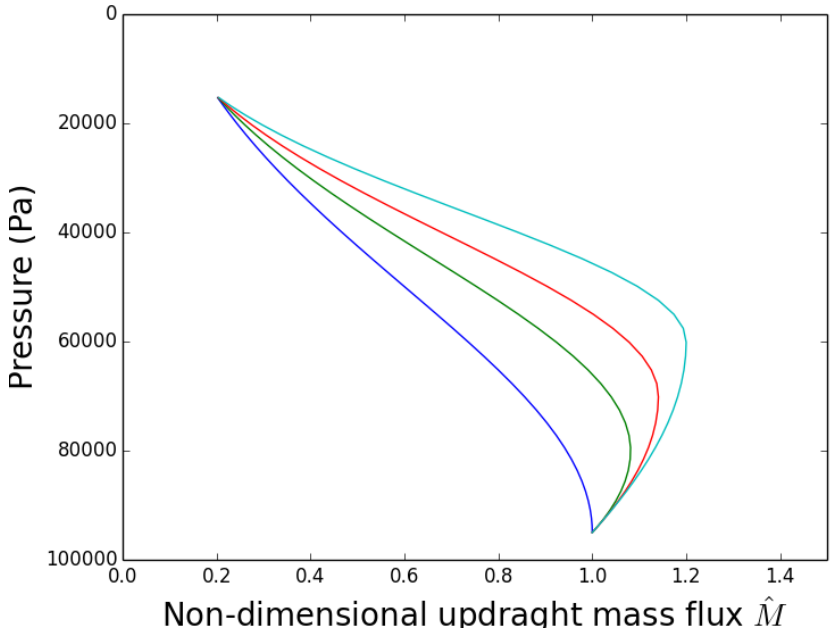

Figure 2: Example of non-dimensional updraught mass flux profile as a function of the pressure of the freezing level. The pressure of the cloud base and cloud top are respectively 95000 Pa and 15000 Pa; $p_{fl} = 96000$ Pa (blue line), $p_{fl} = 80000$ Pa (green line), $p_{fl} = 70000$ Pa (red line) and $p_{fl} = 60000$ Pa (cyan line).

the maximum value of the non-dimensional updraught mass flux $\hat{M}_{max}$ is taken to be:

$$\hat{M}_{max} = \begin{cases} 1 + a_1 \dfrac{(p_{cb} - p_{min}) - p_{fl}}{(p_{cb} - p_{min}) - p_{ref}} & \text{if } p_{fl} \geq p_{ref} \\ 3a_1 & \text{if } p_{fl} < p_{ref} \end{cases}$$

where $p_{ref} = 600$ hPa is a reference pressure and a_1 = 0.5. In (3) we have $\hat{M}_{max} = 1$. β_1 and β_2 in Eqs. (2-3) are chosen so that $\hat{M} = 1$ at cloud base and $\hat{M} = a_2 = 0.2$ at cloud top. This implies $\beta_1 = \ln(\hat{M}_{max})$ and $\beta_2 = \ln(\hat{M}_{max}/a_2)$. The dimensional mass flux at each pressure level is given by:

$$M_k = M_{cb}\hat{M}_k \tag{4}$$

where the cloud base mass flux, M_{cb}, is estimated in the following section.

Examples of the variation in the non-dimensional mass flux profiles with changes in the pressure of the freezing level are shown in Figure 2.

The reliability of Eqs. (2-3) is verified by benchmarking 1188 mass flux profiles against those provided by a 1-dimensional version of the Unified Model, the so called Single Column Model (SCM). The SCM was forced using data from the Tropical Warm Pool–International Cloud Experiment (TWP-ICE) aircraft campaign around Darwin, Australia, over the period from 20 Jan 2006 to 13 Feb 2006. The campaign was aimed at describing the properties of tropical cirrus and the convection that leads to its formation (see [27] for more details). As illustrated in [24], the match

between the profiles is satisfactory, with the empirical formulas providing smoother profiles yet still capturing the majority of the peaks.

2.2.4 Evaluation of the cloud base mass flux

For NWP convective parametrization schemes (e.g. [9]), it is common practise to use the Convective Available Potential Energy (CAPE) as a closure method to estimate the cloud base mass flux. As CAPE is not available as an input field to NAME, in this instance the amount of convective precipitation at the ground is taken as a valid alternative to represent the convective activity inside the cloud with a reasonable approximation.

The integral of the mass fluxes over the depth of the cloud, I (Pa^2/s), is calculated as:

$$I = \int_{p_{ct}}^{p_{cb}} M(p)dp \approx \frac{M_{cb}}{2} \sum_{k=1}^{k_{max}-1} (\hat{M}_k + \hat{M}_{k+1})(p_k - p_{k+1}). \tag{5}$$

Applying statistical regression to the mass fluxes obtained with the SCM from the TWP-ICE field campaign, it is found that a linear relation exists between I and the convective precipitation amount at the ground (available from the SCM forced with TWP-ICE campaign data):

$$I \approx fR \tag{6}$$

where R (kg m^{-2}s^{-1}) is the convective precipitation rate at the ground and $f = 5.9602 \times 10^7$ kg s^{-4} is a conversion factor. The regression line is constrained to go through the origin and is shown in Figure 3. Rearranging Eq. (5) and Eq. (6), it follows that $M_{cb} = 2fR/\sum_k(\hat{M}_k + \hat{M}_{k+1})(p_k - p_{k+1})$, which can then be used to calculate M_k according to Eq. (4). Note that, although the regression is a good fit to the SCM data, we do not expect the regression to be an especially accurate representation of reality. For example, it is possible to have weak convection without precipitation at the ground. The use of Eq. (6) means that the mixing effects of such convection will not be included in the parametrization.

2.2.5 Entrainment and detrainment fluxes

To complete the scheme, entrainment and detrainment fluxes must also be estimated.

The entrainment flux is calculated from the entrainment rate ϵ, which is defined as the rate at which air from the environment is drawn into the cloud through its sides, as a fraction of the updraught mass flux per unit change in pressure:

$$E_k = \epsilon M_k(p_k - p_{k+1}). \tag{7}$$

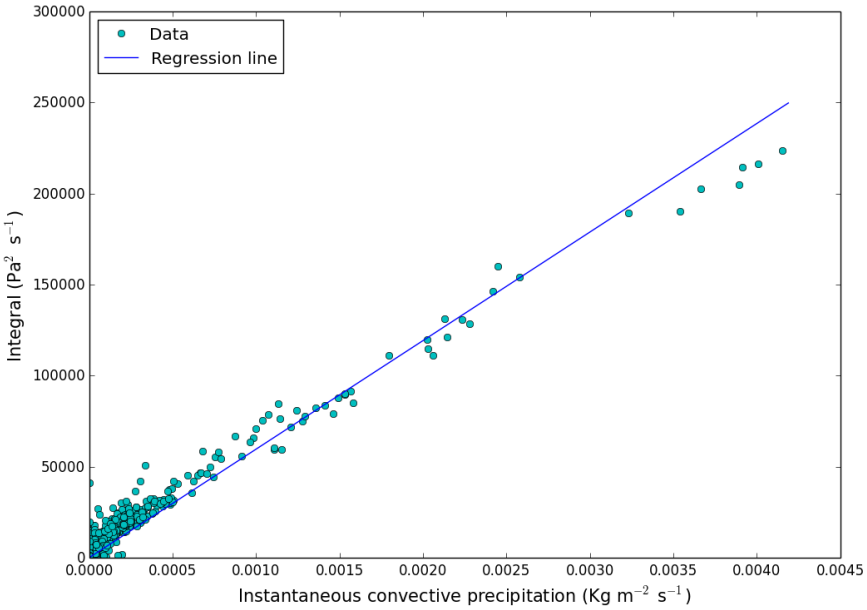

Figure 3: The regression of integrated mass flux I against convective precipitation rate R considered in Eq. (6).

The entrainment rate is estimated as

$$\epsilon = f_{dp} 3 A_E \left(\frac{p_k}{p_0^2} \right) \tag{8}$$

where p_0 is the surface pressure, f_{dp}=0.9 and A_E=1.5, following a similar approach to that in the UM (see also [15] and [32]). It is worth noting that several studies have been undertaken to determine the entrainment rate associated with convective plumes and there is still uncertainty as to what is the best choice of parameters in Eq. (8). Generally a much larger entrainment flux/rate is needed for the pressure layer that includes the cloud base.

The detrainment flux, D_k, is then estimated using eq. 1 after calculating M_k, M_{k+1} and E_k:

$$D_k = M_k + E_k - M_{k+1}. \tag{9}$$

Whenever a negative detrainment flux is encountered, a correction is made to enforce zero detrainment and to increase the entrainment flux in the corresponding pressure layer. Figure 4 illustrates an example of the resulting profiles of mass, entrainment and detrainment fluxes. The largest entrainment flux occurs in the pressure layer containing the cloud base, whilst the detrainment flux has a maximum in the layer including the top of the cloud. Zero detrainment is assumed in the layer containing the cloud base. Including any such detrainment could only detrain material that had just been entrained and so would have little effect. Similarly there is zero entrainment in the layer containing the cloud top.

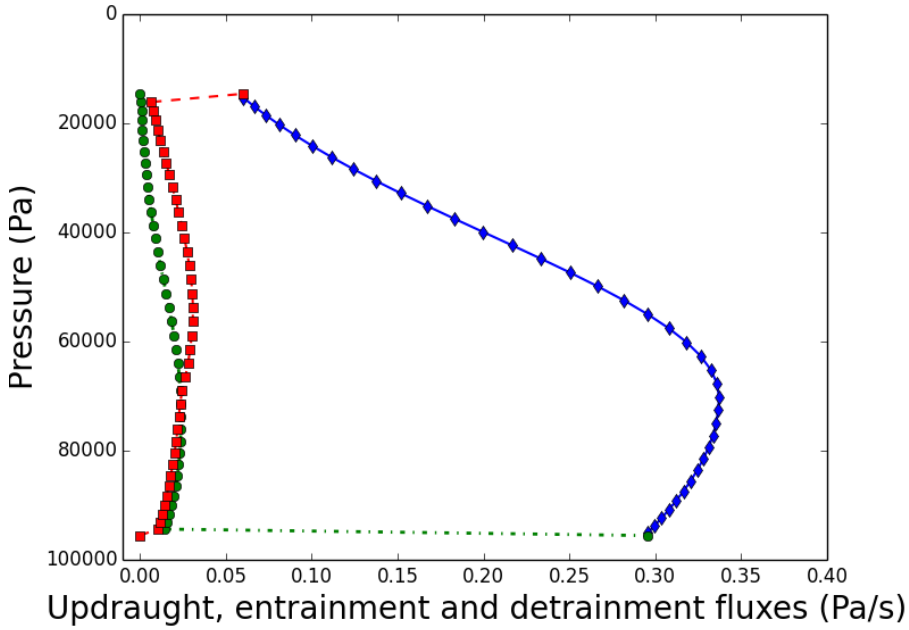

Figure 4: Example of flux profiles as a function of pressure for a cloud base and top of respectively 95000 Pa and 15000 Pa. The fluxes are: updraught mass (blue curve), entrainment (green curve) and detrainment (red curve).

2.2.6 Vertical displacement induced by moist convection

The scheme implemented for upward vertical transport, based on the mass, entrainment and detrainment fluxes, is similar to the one described in [6] for convective transport of chemical species. The probability of a particle entraining into the cloud is calculated as the ratio of the mass of air entraining over the time step divided by the mass of air in the layer. Once entrained, the probability of a particle moving upwards in the updraught to the next layer is evaluated by estimating the fraction of mass that moves upwards with respect to the mass that enters into the cloud layer. Once a particle has entrained into the cloud it can move through a number of pressure layers in a single time step before being brought back to the environment. The probability of detrainment is calculated in a similar way.

For particles in layer k, the probabilities of entraining into the cloud and, if they are already within the cloud, of moving up to the next layer or of detraining are given by

$$P_{ent,k} = \frac{\Delta t E_k}{\Delta p}, \qquad P_{up,k} = \frac{M_{k+1}}{(M_k + E_k)}, \qquad P_{det,k} = 1 - P_{up,k}. \tag{10}$$

where Δt is the model timestep and Δp is the depth of the equally sized pressure layers. For example, $P_{ent,k}$ represents the weight of air entraining ($\Delta t E_k \Delta x \Delta y$) divided by the weight of air in the layer ($\Delta p \Delta x \Delta y$), assuming hydrostatic balance. The resultant motion will be consistent with the mass fluxes assumed, provided that the timestep is small enough to ensure that $P_{ent,k} < 1$ (this condition being satisfied in long range NAME runs where typically $\Delta t(s) \in$[300 : 900]).

To compensate for upward motion, a downward subsidence flux equal to the updraught flux is applied, so that the net flux of air implied by the parametrization is zero and the mean flow isn't altered from the value resolved by the driving NWP model. This subsidence is applied to all particles and the resulting particle height expressed in term of pressure (p_{new}) is calculated as:

$$p_{new,i} = p_{old,i} + M_i \Delta t \tag{11}$$

where M_i is obtained by interpolating the updraught upper and lower level mass fluxes to the i-th particle position and $p_{old,i}$ is the particle position (in pressure) before subsidence is applied.

It is also possible to conduct NAME simulations with the convective parametrization in backward-time mode. In this case, upward vertical displacement by convection is suppressed and replaced by downward vertical displacement. This is obtained by using the updraught mass fluxes as down-draught mass fluxes and the entrainment and detrainment fluxes for updraughts as detrainment and entrainment fluxes for downdraughts, i.e.:

$$M_k^d = M_k; \qquad E_k^d = D_k; \qquad D_k^d = E_k \tag{12}$$

where M_k, D_k and E_k are the updraught mass, entrainment and detrainment fluxes and the super-script d denotes the fluxes associated with the backwards-time downdraught.

Once the fluxes have been calculated, this information is used to estimate how many particles entrain into a given cloud layer and, once entrained, how many particles move downwards and eventually detrain to the environment through a set of probabilities. As in Eq. (10), such probabilities are defined as:

$$P_{ent,k}^d = \frac{\Delta t E_k^d}{\Delta p}, \qquad P_{down,k}^d = \frac{M_k^d}{(M_{k+1}^d + E_k^d)}, \qquad P_{det,k}^d = 1 - P_{down,k}^d. \tag{13}$$

It must be noted that the mass flux index in the estimation of $P_{down,k}^d$ is different from that of $P_{up,k}$ in Eq. (10) due to the different direction of motion. This also means that the probability of detrainment from a vertical downdraught is zero in the top layer of the cloud and, accordingly, the probability of entrainment in a vertical downdraught is zero in the bottom layer of the cloud (the opposite is clear for upward motion as it follows from Eq. (10)). Both entrainment and detrainment fluxes are generally non-zero at intermediate cloud layers. As is the case for upward motion, once a particle has entrained into the cloud it can jump through several pressure layers before being brought back to the environment.

Lastly, an upward flux is applied to compensate for the downdraught motion (this is the subsidence flux discussed above but viewed backwards in time), and the resulting particle pressure is made smaller according to the following equation:

$$p_{new,i} = p_{old,i} - M_i^d \Delta t \tag{14}$$

where M_i^d is obtained by interpolating the upper and lower level mass fluxes to the i-th particle position.

3 Consistency of the scheme with exact results

3.1 Backward-forward probability distributions

Atmospheric dispersion models are often used to give predictions of particle concentration by estimating the forward-time conditional probability density distribution at ($\mathbf{x}$, t) for particles released at ($\mathbf{x}_0$, t_0), i.e. $P^f(\mathbf{x}, t|\mathbf{x}_0, t_0)$, or the backward-time conditional probability $P^b(\mathbf{x}_0, t_0|\mathbf{x}, t)$ at ($\mathbf{x}_0$, t_0) for particles released at ($\mathbf{x}$, t). As shown in [12], Bayes' theorem on conditional probability leads to:

$$P^b(\mathbf{x}_0, t_0|\mathbf{x}, t) = \frac{\rho_a(\mathbf{x}_0, t_0)}{\rho_a(\mathbf{x}, t)} P^f(\mathbf{x}, t|\mathbf{x}_0, t_0) \tag{15}$$

where $\rho_a(\mathbf{x}_0, t_0)$ and $\rho_a(\mathbf{x}, t)$ are the unconditional probability density for a fluid element to be at $(\mathbf{x}_0, t_0)$ and $(\mathbf{x}, t)$. In addition, if we use pressure as the vertical coordinate (as in the convection scheme) with concentrations and densities defined as kg m^{-2} Pa^{-1} and probability densities as the probability per unit volume with volume defined as m^2 Pa, then the hydrostatic approximation implies $\rho_a = 1/g$ where g is the gravitational acceleration and so eq. 15 becomes $P^b(\mathbf{x}_0, t_0|\mathbf{x}, t) = P^f(\mathbf{x}, t|\mathbf{x}_0, t_0)$.

The forward-backward equivalence can thus be used to test the robustness of the convection scheme although an exact equivalence cannot be expected in the realm of numerical modelling with finite Δt. An idealised test case is set up over subequatorial Africa to ensure the presence of convective precipitation and convective clouds of significant vertical development [18]. To isolate the effect of convection from any other atmospheric effects, advection by mean wind and diffusion by turbulence are suppressed. In addition, meteorological variables provided as input at the grid nodes are kept fixed both in space and time. Details of the simulation are given in Table 1; essentially it is a 1-dimensional simplified model in which particles released instantaneously can only be displaced vertically due to the effect of atmospheric moist convection.

This simulation setting is then used to test the forward/backward equivalence in the following way. 10 pressure layers (11 pressure levels) are defined with $p_1 = 51387$ Pa (below the cloud base), $p_{11} = 28186$ Pa (just above the cloud top) and $\Delta p = 2320.1$ Pa. First, 10 forward simulations are performed, with, in the ith simulation, all particles released uniformly between p_i and p_{i+1}, $i \in [1, 10]$, and tracked for 21 hours according to the start and end time in Table 1. The total number of particles per layer is then recorded at the end of each simulation, resulting in a 10 $\times$ 10 matrix where columns indicate the layer within which particles are released and rows the destination layer.

Then, the same procedure is repeated for backward runs (see Table 1). Finally, the forward matrix and the transpose of the backward matrix are compared by calculating the difference (as a

Table 1: Details of NAME simulations to test the forward/backward probability equivalence described in section 3a.

Parameter name (and unit)	Parameter value
No. particles	2,000,000
Release location (Lat,Long)	21.22W, 16.02S
Convective precipitation (mm/hr)	0.1496431
Freezing level (Pa)	56773.37
Convective cloud base (Pa)	50227.0
Convective cloud top (Pa)	29346.1
Δp (Pa)	2320.1
Fwd start time	01/12/2015 03:00 UTC
Fwd end time	02/12/2015 00:00 UTC
Bwd start time	02/12/2015 00:00 UTC
Bwd end time	01/12/2015 03:00 UTC
Δt (s)	300

Table 2: Percentage difference in particle numbers per pressure layer between the forwards and backwards simulations, calculated by subtracting the transpose of the backwards matrix from the forwards matrix and dividing by the total number of particles of the simulation. Columns indicate the release layer number and rows the destination layer number.

		Release layer									
		1	2	3	4	5	6	7	8	9	10
	1	1.17	1.75	1.39	1.47	1.69	0.98	0.00	0.00	0.00	0.00
	2	0.58	0.17	1.00	0.93	0.75	1.02	-0.73	0.00	0.00	0.00
	3	0.23	1.56	0.09	0.64	0.57	0.32	-0.21	0.00	0.00	0.00
	4	0.51	-0.51	1.14	-0.03	0.29	0.13	0.50	-0.70	0.00	0.00
End	5	-0.21	1.22	-0.23	0.51	-0.11	-0.02	-0.16	-0.19	0.00	0.00
layer	6	0.31	-0.73	0.07	0.28	-0.26	-0.21	-0.21	0.29	-0.45	0.00
	7	-0.88	0.55	0.72	-1.01	0.26	-0.31	-0.20	-0.20	-0.17	0.00
	8	-1.80	-1.95	-2.10	-0.27	-0.24	-0.69	-0.46	-0.45	-0.17	-0.64
	9	-0.71	-0.55	-0.88	-1.73	-2.49	-1.02	-0.52	-0.55	-0.53	-0.78
	10	0.73	0.92	0.83	0.76	0.56	0.20	-0.08	-0.06	-0.12	-0.52

percentage) between the number of particles in each matrix element divided by the total number of particles of the simulation; the result is shown in Table 2. The mean of the absolute values in Table 2 is 0.54% and the standard deviation is 0.76% indicating a good level of agreement between the two matrices. Although not shown here, the statistical equivalence between the forward and backward runs improves with reduced timestep size (which in turn increases the computational time of the simulation).

3.2 The well-mixed condition

Another pivotal criterion that atmospheric dispersion models aim to fulfil is the so called “well-mixed condition”: particles which are well-mixed at an initial time t_0 (in our case that means distributed uniformly in pressure in the vertical) should remain well-mixed. It can be proved that the well-mixed condition follows from the forward-backward equivalence by adapting the derivation given by [33] to

the type of model considered here. If starting with a well mixed distribution, e.g. concentration = 1 g m^{-2} Pa^{-1}, then the concentration at time t is $\int P^f(\mathbf{x}, t|\mathbf{x}_0, t_0)dx_0 = \int P^b(\mathbf{x}_0, t_0|\mathbf{x}, t)dx_0 = 1$, where the last equality is a consequence of $P^b(\mathbf{x}_0, t_0|\mathbf{x}, t)$ being a probability density function. Figure 2 in [24] illustrates how the well mixed state is approached over time for a forward simulation which starts away from the well-mixed state.

4 Assessment of the performance of the new parametrization scheme of convective transport

In this section two case studies are presented and discussed. The aim here is to assess whether the new scheme provides a realistic representation of particle transport when moist convection is significant. The first case study is designed to investigate how the new parametrization of convection influences the particle transport and to assess whether it gives a qualitatively correct treatment of convection which is likely to enhance the performance of NAME. In the second case study we make a more quantitative assessment of the concentration predictions against observations of methyl iodide. In both cases we consider the results from NAME both with the new convection scheme and without a convection scheme. This makes it easier to see what the scheme is doing than would be possible by comparing the new and old schemes.

The search for a suitable set of measurement data to compare with the model has proved to be particularly challenging. The ideal setting to quantify whether a model is reproducing the convectively-induced displacement of particles to a reasonable approximation requires data on either a controlled-release tracer or on a natural tracer with an atmospheric lifetime (or a limited emission period) that makes the tracer concentration field sensitive to tropospheric convection. We also need known sources and emission rates and measurements throughout the troposphere up to the lower stratosphere (where the highest convective cloud tops are found) over a region of the globe where the frequency of moist atmospheric convection is high. Finally the chemical and deposition characteristics should be simple – ideally the tracer should be inert except perhaps for a simple exponential decay in order to avoid complications from other factors.

To the best of the authors' knowledge, a set of measurement data satisfying such requirements does not exist. In [13], model results were compared against two large-scale tracer experiments (CAPTEX and ANATEX) and it proved difficult to draw clear conclusions on the performance of the convective parametrization scheme for a number of reasons described in their paper which would also apply to this study. In the same paper, the authors also used observations of the radon 222 isotope provided by aircraft campaigns in 1993 and 1994, but due to uncertainties in the radon emissions and problems in making accurate predictions near steep radon 222 gradients in the atmosphere, the comparison between modelled and observational data proved to be hard. In our second case study we explore using a recent set of observations from the ATTREX campaign [20]

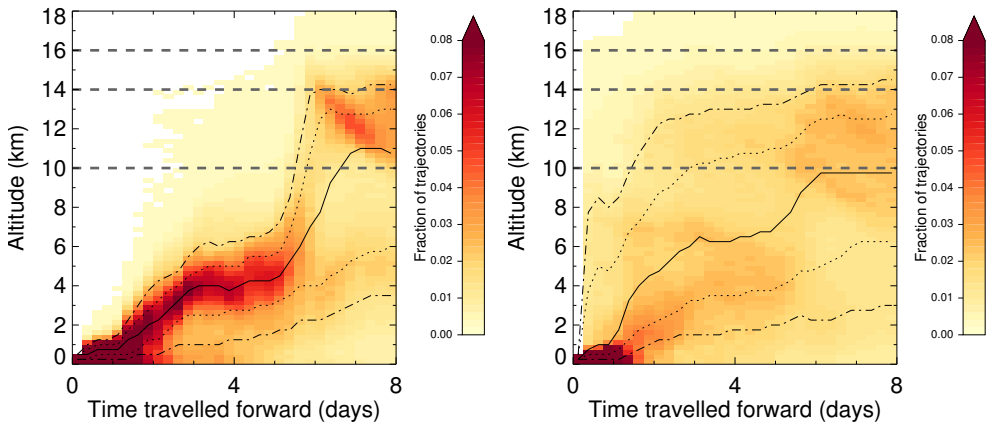

(a) without convection (b) with convection

Figure 5: Particle height distribution every 6 hours expressed as the fraction of trajectories per 0.25 km altitude range for the forwards NAME simulation (a) without a convection parametrization and (b) with the new convection parametrization. The solid, dotted, and dash-dot black lines mark the median, the 25th and 75th percentiles, and the 10th and 90th percentiles of the trajectory altitude. The straight dashed lines show the threshold heights used in Table 3.

involving methyl iodide which is released primarily from marine waters. The atmospheric lifetime of methyl iodide is comparable to the half life of radon 222, making its upper troposphere concentrations similarly sensitive to convective mixing.

4.1 Illustration of the convective parametrization over the West Pacific

We illustrate the effect of the convective parametrization over the Tropical West Pacific Warm Pool region, well known for its high sea surface temperatures and the rapid and intense nature of convective events [17]. 100,000 inert particles were released instantaneously in NAME at 12:00 UTC on 21st January 2016 at 160°E, 0°N within a box of dimension $0.5° \times 0.5°$ between 200 and 300 m asl, i.e. within the marine atmospheric boundary layer. NAME was driven by the three dimensional meteorological fields from the Met Office Unified Model at a spatial resolution of 0.234° longitude by 0.156° latitude with 59 vertical levels up to 29 km and a temporal resolution of 3 hours. Particles were tracked for 8 days forwards in time to identify the time required for trajectories to reach the upper troposphere, with and without the new convection scheme. An otherwise identical simulation was also conducted in which the particles were tracked backwards in time from a source centred on 14000 m asl.

Figure 5 shows the evolution of the particle distribution in the vertical for the forwards simulation, with and without the new convection scheme. The convection scheme clearly makes an appreciable difference. With convection, a higher fraction of particles reside in the upper troposphere during the first days of the simulation. Without convection, the bulk of the particles stay in the lower troposphere (0-6000 m asl) up to the end of day 5 of the simulation and only after that are particles found in high concentration between 10 and 14 km asl.

Table 3: Percentage of particles crossing above a given altitude (10, 14 and 16 km asl) at some time during the forwards simulation, and percentage crossing below a given altitude (8, 5 and 1 km asl) during the backwards simulation. Results are shown both without a convection parametrization and with the new convection parametrization.

	Forwards			Backwards		
Thresholds (km)	10	14	16	8	5	1
without convection	60.7	23.1	2.1	49.3	29.0	8.1
with convection	70.7	26.6	5.8	73.0	62.4	38.7

The percentage of particles which travel above 10, 14 and 16 km asl are shown in Table 3 and Figure 6 shows the distribution of the time at which particles first cross 10 km. The 10 km threshold approximately represents the upper troposphere, which is where the maximum convective outflow takes place [28]; 14 km is a reasonable approximation to the level of zero net radiative heating, a transition area between the tropospheric-like convective lower Tropical Tropopause Layer (TTL) and the stratospheric-like radiative upper TTL, the two dynamical transport regimes in the TTL; and 16 km is in the upper TTL. These altitude thresholds are highlighted with straight dashed lines in Figure 5.

The use of the convection parametrization leads to a higher fraction of particles being displaced above 10 km during the run. Without the convective parametrization, almost no particles are uplifted to the upper troposphere during the first half of the simulation, while a significant upward flux of particles occurs around day 6 (see Figure 6 (a)). However, with the parametrization included, 3 uplift peaks occur, with the last one coinciding with the time of the uplift peak in Figure 6 (a). At the times of the uplift peaks, the plume of particles lies inside a tropical equatorial system of very deep convective clouds whose vertical extent exceeds 10 km with tops up to 18 km asl (according to the data from the UM). Therefore, the vertical displacement of particles with the convective parametrization between day 0 and day 4 of the simulation is very plausible, and the lack of uplift above 10 km during this period in the case without the convection parametrization is likely to be a considerable underestimate of particle vertical transport.

To investigate why the peak uplift at about 27/01/2016 00:00 UTC also occurs without the convection parametrization, we looked at the resolved vertical velocity from the UM averaged over 167°E to 173°E and 12°S to 6°S. This region was chosen to include the bulk of the locations where particles move above 10 km for the first time between 26/01/2016 12:00 UTC and 27/01/2016 12:00 UTC. At the time of the particle uplift in Figure 6 (b), there is an increase in the resolved vertical velocity with a peak of order 0.2 m s^{-1} at around 10 km, which explains the presence of the uplift peak without the convection parametrization.

Figure 7 shows the particle vertical distribution for the backwards simulation, with and without the convection scheme. The percentage of particles which travel below 8, 5 and 1 km is shown in Table 3, with these altitude thresholds marked with straight dashed lines in Figure 7. The thresholds correspond to levels in the mid troposphere (8 and 5 km) and roughly to the marine atmospheric

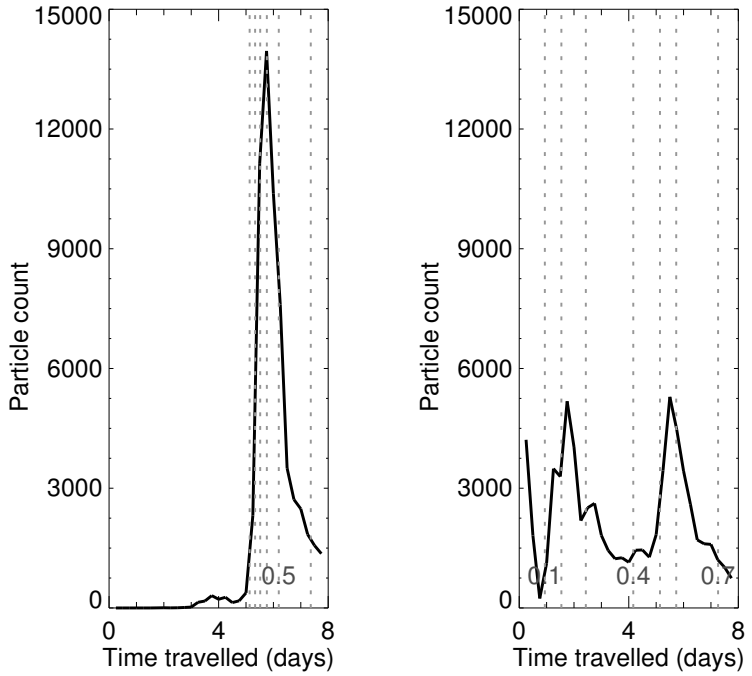

(a) without convection (b) with convection

Figure 6: The number of particles crossing above 10 km asl for the first time in each 6 hour interval for the forwards NAME simulation (a) without a convection parametrization and (b) with the new convection parametrization. The straight dashed lines show the times when the cumulative fraction of particles which have crossed 10 km increases by 0.1.

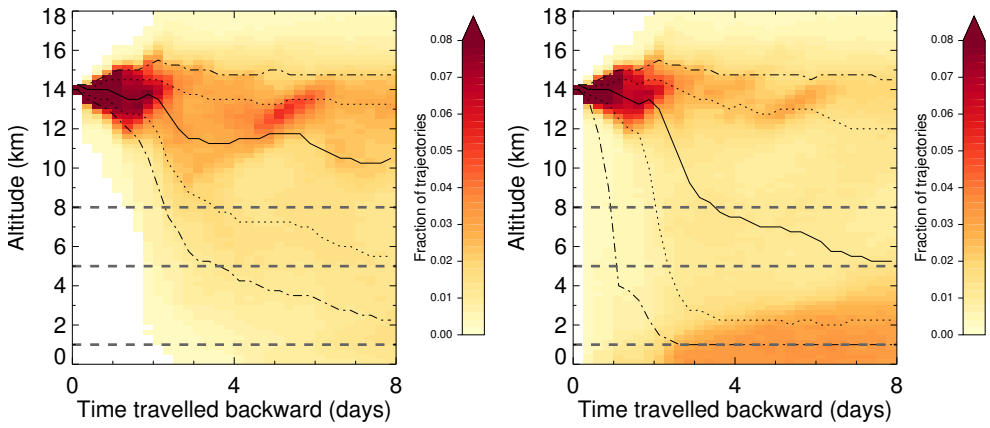

(a) without convection (b) with convection

Figure 7: As Figure 5 but for the backwards NAME simulation.

boundary layer (1 km). Once again, there is a clear difference between the results with and without the parametrization of convection, with the parametrization moving material from the top to the low troposphere faster and in a more efficient manner.

4.2 Comparison with ATTREX Research Flights

The NASA Airborne Tropical TRopopause EXperiment (ATTREX) included a flight campaign in early 2014 (January-March) during which the unmanned Global Hawk aircraft made atmospheric measurements throughout the western Pacific Tropical Tropopause Layer (see [20] for an extensive description of the campaign). The large number of in situ measurements made during the 8 research flights and their subsequent analysis has provided a wealth of information on the presence and transport pathways of halogenated very short-lived substances, e.g. [25] and [1]. Here we focus on the flights with the most convective conditions, namely flights RF02, RF03, RF04 and RF05.

One of the chemical compounds measured during the flights is methyl iodide (CH_3I). Methyl iodide is primarily released by marine waters ([29] and [3]) and has an atmospheric lifetime of a few days, with the primary removal route being by photolysis. The mean lifetime of the species is estimated as 4 days ([5] and [4]). As a result it will only be found in significant quantities in the TTL if it has recently experienced fast upward transport from the atmospheric boundary layer. It is thus a good tracer for convection. Methyl iodide was measured during the flights using the Advanced Whole Air Sampler (AWAS); for details of the AWAS instrumentation see section 2.2.3 of [1].

During the same period (early 2014) and in the same region (western Pacific) CH_3I was also measured at altitudes below 14 km by the NCAR Gulfstream-V High-performance Instrumented Airborne Platform for Environmental Research and by the NERC BAe-146 Facility for Airborne Atmospheric Measurements, as part of the CONTRAST (CONvective TRansport of Active Species in the Tropics) and CAST (Coordinated Airborne Studies in the Tropics) experimental campaigns

[26, 16, 1]. These measurements are not considered in detail here except to estimate boundary layer concentrations.

Figure 8 (a) shows the measured vertical distribution of methyl iodide. According to the measurements, the mean concentration of CH_3I smoothly decreases from a mean value of $\sim$0.24 ppt between 14 and 15 km asl to $\sim$0.05 ppt between 17 and 18 km asl.

NAME simulations were performed backwards in time from each measurement sampling location to estimate which areas of the marine atmospheric boundary layer had contributed air to the sampling location, and how long ago the contributing air had left the boundary layer. The concentration of CH_3I (expressed as a volume mixing ratio) at the receptor at time t, $C(\mathbf{x}, t)$, was then estimated assuming an exponential decay of CH_3I [2]:

$$C(\mathbf{x}, t) = \langle C(\mathbf{x}_0, t_0) \exp(-t/\tau) \rangle \approx C(\mathbf{x}_0, t_0) \sum_{i=1}^{N_t} f(i) \exp(-t_i/\tau). \quad (16)$$

Here $\langle\ \rangle$ indicates an average over particles, τ is the mean lifetime of the species for which we use the estimate of 4 days given above, and t is the time before the measurement time that the particle was last below 1 km (taken as infinite for particles which do not go below 1 km during the simulation). The initial concentration $C(\mathbf{x}_0, t_0)$ was taken to be 0.696 ppt. This is the mean value measured below 1 km by the CONTRAST and CAST experiments in the same region and during the same period as the ATTREX experiment. It is also similar to the values for the mixing ratio of methyl iodide in the marine atmospheric boundary layer given in Table 1.7 of [4] (median 0.8 ppt and range 0.3-2.1 ppt). In practice $C(\mathbf{x}, t)$ is evaluated via the right hand expression in (16) where i is the timestep, N_t the number of timesteps and $f(i)$ is the fraction of particles found below 1 km for the first time (going backwards) at the end of timestep i.

Figure 8 (b) and (c) show the modelled concentration of methyl iodide according to Eq. (16) where $f(t)$ is found by running NAME backwards for 12 days with and without the new convection scheme. The motivation for choosing a simulation time of 12 days is to be able to capture the sources of CH_3I in the atmospheric boundary layer. The amount of CH_3I contributed by older air is likely to be small because 12 days $\gg \tau$. Clearly, the simulation with the convection scheme, Figure 8 (b), leads to a larger estimate of the average concentration of CH_3I at heights above 14 km asl than the simulation without convection, Figure 8 (c). The observations and the simulation with convection are consistent in indicating that the composition of air in the 14-15 km range has a strong contribution from 'fresh' air masses recently lofted from the boundary layer with a typical implied age of order τ. The implied age increases with altitude.

As shown in Table 4, the simulation with convection shows a better statistical match with the measured concentrations (Figure 8a) than the simulation without convection. With the convection scheme, the magnitudes of the CH_3I concentrations are correct at the bottom of the TTL, indicating that the convection scheme is, on average, transporting the correct amount of air from the boundary layer to the TTL. However, although the convection scheme improves the concentrations at all

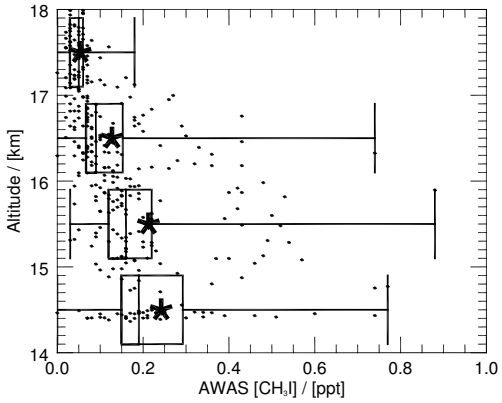

(a) Flight measurements

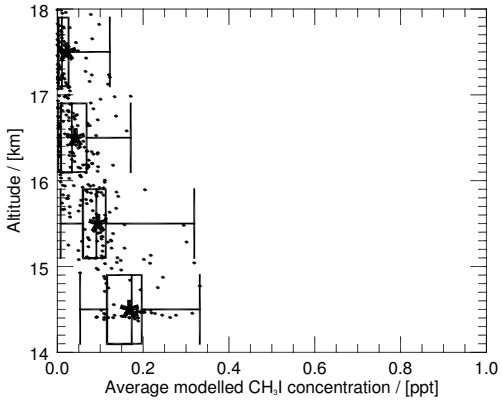

(b) NAME predictions with convection

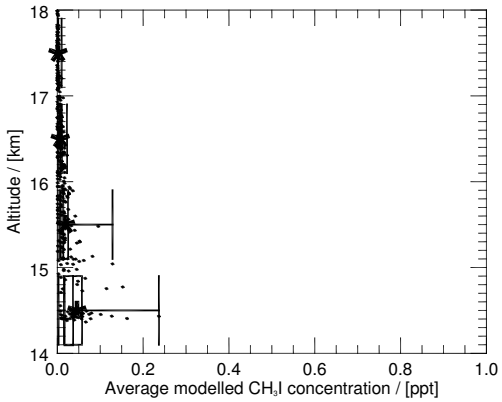

(c) NAME predictions without convection

Figure 8: Concentration of methyl iodide in the TTL from the four ATTREX 2014 flights RF02-5 combined, showing the flight measurements and the corresponding NAME predictions with and without the scheme for parametrization of convection. The boxplots show the median, lower and upper quartile, minimum and maximum for those measurements/predictions which fall in each 1 km layer. The mean for each layer is marked with a star symbol and the dots show the individual values.

Table 4: Mean (and standard deviation in parentheses) over various atmospheric altitude ranges of the CH_3I concentrations calculated from the AWAS measurements collected during ATTREX 2014 flights RF02-5 and from estimates obtained at the same locations and times using Eq. (16) and NAME, both with and without the scheme for parametrization of convection.

		NAME predictions	
Altitude (km)	AWAS measurements (ppt)	with convection (ppt)	without convection (ppt)
17-18	0.05 (0.03)	0.02 (0.02)	0.00 (0.00)
16-17	0.13 (0.07)	0.04 (0.03)	0.01 (0.00)
15-16	0.20 (0.09)	0.09 (0.04)	0.02 (0.02)
14-15	0.24 (0.13)	0.17 (0.06)	0.05 (0.04)

the heights considered, the performance decreases with height with a tendency to underestimate the concentration at the higher heights, indicating that the transport to higher heights is underpredicted. Possible explanations are that convection in the UM (which are inputs to the convection parametrization) may not reach high enough, that smaller scale turbulence, perhaps associated with jets, plays a role, that material which left the boundary layer more than 12 days ago makes a significant contribution (12 day old air would have a concentration of 0.035 ppt), and/or that the NAME mass fluxes are not large enough near the cloud tops. There is some independent evidence suggesting that the UM tends to underestimate the depth of the deepest convection in the tropics – see e.g. comparisons with CALIPSO satellite data in figure 5 of [36] (although both model curves in that figure are from slightly later versions of the UM).

In Figure 9 the measurements and NAME predictions with the convection parametrization for the individual flights are shown. Flight RF02 (16th-17th February) was forced to remain within line of sight and survey a single location due to a faulty communication instrument onboard the aircraft. As a result multiple vertical profiles in the TTL were collected over the east coast of Guam, Micronesia, during the 17 hours of the flight, including measurements in cirrus outflows from convection. In flight RF03 (4th-5th March) the cirrus outflow from tropical cyclone Faxai was sampled north of Guam. Flight RF04 (6th-7th March) surveyed the western Pacific encountering air which had been influenced by convection several days previously. The last flight considered here, flight RF05 (9th-10th March), flew south east of Guam encountering strong convection associated with tropical cyclone Lusi. Further details on these flights are presented by [20].

The NAME predictions for flight RF02 are quite good at 14 km, but this flight shows the tendency to underpredict at higher heights most clearly. On flight RF03, very high values of CH_3I were measured which are not captured by NAME. However the profile shape is better with the concentrations from NAME not falling off as fast with height as for RF02. For flights RF04 and RF05 the agreement between NAME and the measurements is rather good. We have not shown predictions for the individual flights without the convection parametrization. However in all cases the predictions with the parametrization are much better than without.

Further analysis of these and other similar measurements is presented in [11]. This includes

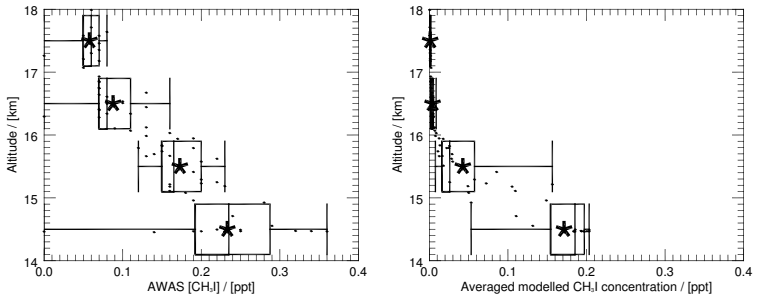

(a) Flight RF02, measurements (b) Flight RF02, NAME predictions

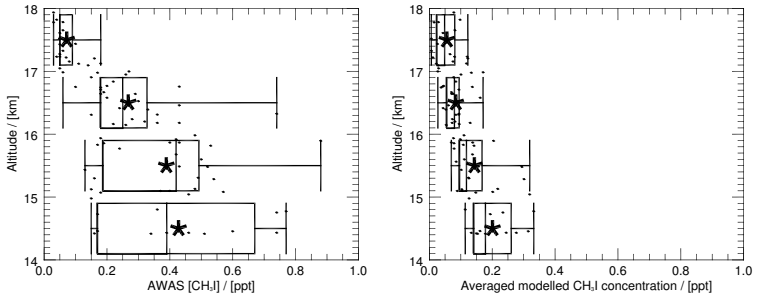

(c) Flight RF03, measurements (d) Flight RF03, NAME predictions

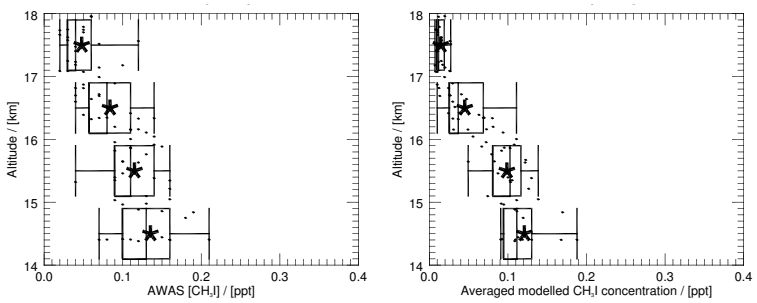

(e) Flight RF04, measurements (f) Flight RF04, NAME predictions

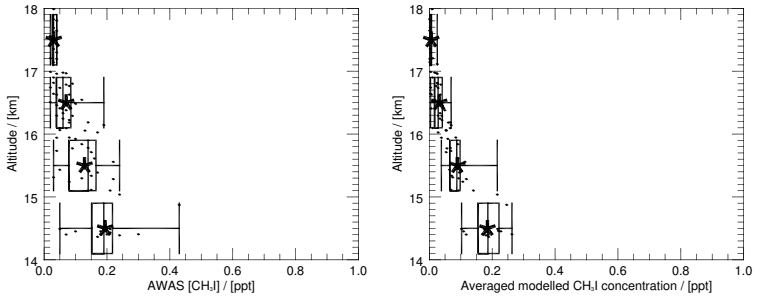

(g) Flight RF05, measurements (h) Flight RF05, NAME predictions

Figure 9: Concentration of methyl iodide in the TTL from the four ATTREX 2014 flights RF02-5 separately, showing the flight measurements and the corresponding NAME predictions with the scheme for parametrization of convection. The boxplots show the median, lower and upper quartile, minimum and maximum for those measurements/predictions which fall in each 1 km layer. The mean for each layer is marked with a star symbol and the dots show the individual values.

analysis of other flights with less convective influence where the measured concentrations of CH_3I are rather lower, with NAME also predicting appropriately low values. Background concentrations from material which has not recently been in the boundary layer are also assessed. A similar analysis of bromoform ($CHBr_3$) and dibromomethane (CH_2Br_2) is performed although these are longer lasting chemicals whose concentration is less sensitive to recently occurring convection.

5 Concluding remarks

The object of this paper is to describe the working principles and the performance of a scheme recently developed in the NAME model to parametrize moist atmospheric convection above the boundary layer. The scheme enables NAME to simulate the convectively-induced transport of airborne pollutants via a probabilistic approach based on mass fluxes which is valid for both forward and backward NAME simulations.

The first part of the paper presents the approach. The method used to estimate the convective updraught, entrainment and detrainment fluxes is described with particular emphasis on the use of convective precipitation rate to estimate the cloud base mass flux. The way the model particles move in response to the mass fluxes is also presented.

An idealised test case (in which both the spatial and temporal variation of meteorological conditions have been suppressed) has been set up to evaluate the forward-backward probability equivalence [12]. In addition, it has been shown that the well-mixed criterion [33] follows from the above mentioned probability equivalence.

A qualitative and quantitative assessment of the performance of the scheme in NAME is carried out in section 4. Two case studies are carried out over the West Pacific region, well known for the presence of intense convective activity. The first case investigates the transport of inert particles instantaneously released over the Equator; separate simulations are carried out to compare the dispersion with the new convection scheme against that without. An analysis shows that the parametrization of convection produces a plausible redistribution of particles across the troposphere, while the lack of such a parametrization leads to a much reduced concentration of particles at higher altitudes for runs in forward mode from a low release, or at low altitudes for runs in backward mode from a high release.

The second case study attempts to validate the results of the NAME simulations obtained with the new scheme against observations. As discussed in section 4, in the context of tropospheric convection the current availability of measurements suitable for benchmarking modelled data against is very limited. In this paper, 351 aircraft observations of methyl iodide obtained during four flights from the recent ATTREX campaign are used. The implementation of the new convective scheme is shown to improve the match between modelled and measured concentrations of CH_3I above 14 km asl.

Although usually the meteorological fields are supplied to NAME by the Met Office NWP model,

the Unified Model, the newly devised convective scheme (as well as NAME) has the flexibility to be used with other NWP datasets as long as convective cloud base, convective cloud top and convective precipitation rate are provided as input. Presently, the mass fluxes used in the new scheme are not provided as input to NAME from the NWP model but are estimated using an empirical approach; this could change if in future a tighter coupling between NAME and the UM takes place.

In its present formulation, the performance of the scheme could possibly be improved by considering downdraughts as well as the existing updraughts for forward-in-time simulations (and vice versa for backward-in-time simulations). The implementation of the new scheme inevitably leads to a higher computational run-time; although it is difficult to provide a general estimate of the increase (as it depends on extent of atmospheric convection) it has not yet been observed to be higher than 5-10%.

The scheme is suitable for use in simulations of long range dispersion when using meteorological fields with a horizontal resolution which is insufficient to capture the existence of convective clouds. In such situations the ability to parametrize the vertical transport by moist convection can be crucial to making accurate dispersion forecasts.

Acknowledgments The authors thank the many colleagues in the Met Office Atmospheric Parametrizations and Processes group for fruitful discussions about convection in the UM and in particular Ben Shipway for providing data from the TWP-ICE campaign. We acknowledge funding from the Natural Environment Research Council (NERC) Grant NE/J006246/1 for the CAST project and from NASA Grant NNX10AO83A S08 for the work of Maria Navarro and Elliot Atlas.

References

[1] S.J. Andrews, L.J. Carpenter, E.C. Apel, E. Atlas, V. Donets, J.R. Hopkins, R.S. Hornbrook, A.C. Lewis, R.T. Lidster, R. Lueb, J. Minaeian, M. Navarro, S. Punjabi, D. Riemer, and S. Schauffler. A comparison of very short-lived halocarbon (VSLS) and DMS aircraft measurements in the tropical west Pacific from CAST, ATTREX and CONTRAST. *Atmos. Meas. Tech.*, 9:5213–5225, 2016.

[2] M. Ashfold, N. Harris, E. Atlas, A. Manning, and J. Pyle. Transport of short-lived species into the Tropical Tropopause Layer. *Atmos. Chem. Phys.*, 12:6309–6322, 2012.

[3] N. Bell, L. Hsu, D.J. Jacob, M.G. Schultz, D.R. Blake, J.H. Butler, D.B. King, J.M. Lobert, and E. Maier-Reimer. Methyl iodide: Atmospheric budget and use as a tracer of marine convection in global models. *J. Geophys. Res.*, 107(D17):4340, 2002.

[4] L.J. Carpenter, S. Reimann, J.B. Burkholder, C. Clerbaux, B.D. Hall, R. Hossaini, J.C. Laube, and S.A. Yvon-Lewis. Update on Ozone-Depleting Substances (ODSs) and other gases of

interest to the montreal protocol. *Scientific Assessment of Ozone Depletion: 2014, Global Ozone Research and Monitoring Project-Report No.55*, pages 1.1–1.101, 2014.

[5] D.S. Cohan, M.G. Schultz, D.J. Jacob, B.G. Heikes, and D.R. Blake. Convective injection and photochemical decay of peroxides in the tropical upper troposphere: Methyl iodide as a tracer of marine convection. *J. Geophys. Res.*, 104(D5):5717–5724, 1999.

[6] W.J. Collins, R.G. Derwent, C.E. Johnson, and D.S. Stevenson. A comparison of two schemes for the convective transport of chemical species in a Lagrangian global chemistry model. *Quart. J. Roy. Meteor. Soc.*, 128:991–1009, 2002.

[7] M.J.P. Cullen. The unified forecast/climate model. *Meteor. Mag*, 122:81–94, 1993.

[8] R. D'Amours, A. Malo, T. Flesch, J. Wilson, J.-P. Gauthier, and R. Servranckx. The Canadian Meteorological Center's Atmospheric Transport and Dispersion Modelling Suite. *Atmos. Ocean*, 53:176–199, 2015.

[9] S.H. Derbyshire, A.V. Maiden, S.F. Milton, R.A. Stratton, and M.R. Willet. Adaptive detrainment in a convective parametrization. *Quart. J. Roy. Meteor. Soc.*, 137:1856–1871, 2011.

[10] K. A. Emanuel. *Atmospheric Convection*. Oxford University, New York, 1994.

[11] M. T. Filus. *Transport and distribution of the short-lived halocarbons in the tropical tropopause layer in the Pacific Ocean: the role of convection*. PhD thesis, University of Cambridge, 2017.

[12] T.K. Flesch and J.D. Wilson. Backward-time Lagrangian stochastic dispersion models and their application to estimate gaseous emissions. *J. Appl. Meteor.*, 34:1320–1332, 1995.

[13] C. Forster, A. Stohl, and P. Seibert. Parameterization of convective transport in a Lagrangian particle dispersion model and its evaluation. *J. Appl. Meteor. Climatol.*, 46:403–422, 2007.

[14] C. Gardiner. *Stochastic Methods – A Handbook for the Natural and Social Sciences*. Springer, 4th edition, 2009.

[15] D. Gregory and P.R. Rowntree. A mass flux convection scheme with representation of cloud ensemble characteristics and stability dependent closure. *Mon. Weather Rev.*, 118:1483–1506, 1990.

[16] N. R. P. Harris, L. J. Carpenter, J. D. Lee, G. Vaughan, M. T. Filus, R. L. Jones, B. OuYang, J. A. Pyle, A. D. Robinson, S. J. Andrews, A. C. Lewis, J. Minaeian, A. Vaughan, J. R. Dorsey, M. W. Gallagher, M. Le Breton, R. Newton, C. J. Percival, H. M. A. Ricketts, S. J.-B. Bauguitte, G. J. Nott, A. Wellpott, M. J. Ashfold, J. Flemming, R. Butler, P. I. Palmer, P. H. Kaye, C. Stopford, C. Chemel, H. Boesch, N. Humpage, A. Vick, A. R. MacKenzie, R. Hyde, P. Angelov, E. Meneguz, and A. J. Manning. Coordinated airborne studies in the tropics (CAST). *Bull. Amer. Meteor. Soc.*, 98:145–162, 2017.

[17] R.W. Helber and R.H. Weisberg. Equatorial upwelling in the Western Pacific Warm Pool. *J. Geophys. Res*, 106(C5):8989–9003, 2001.

[18] R.A. Houze, K. L. Rasmussen, M.D. Zuluaga, and S. R. Brodzik. The variable nature of convection in the tropics and subtropics: a legacy of 16 years of the Tropical Rainfall Measuring Mission Satellite. *Rev. Geophys.*, 53:994–1021, 2015.

[19] P. Hurley. Development and verification of TAPM. In Borrego C. and Miranda A. I., editors, *Air Pollution Modeling and Its Application XIX*, pages 208–216. Springer, Dordrecht, Netherlands, 2008.

[20] E.J. Jensen, L. Pfister, D.E. Jordan, T.V. Bui, R. Ueyama, H.B. Singh, T.D. Thornberry, A.W. Rollins, R.-S. Gao, D.W. Fahey, Rosenlof K.H, J.W. Elkins, G.S. Diskin, J.P. DiGangi, R.P. Lawson, S. Woods, E.L. Atlas, M.A. Navarro-Rodriguez, S.C. Wofsy, J. Pittman, C.G. Bardeen, O.B. Toon, B.C. Kindel, P.A. Newman, M.J. McGill, D.L. Hlavka, L.R. Lait, M.R. Schoeberl, J.W. Bergman, H.B. Selkirk, M.J. Alexander, J.-E. Kim, B.H. Lim, J. Stutz, and K. Pfeilsticker. The NASA airborne tropical tropopause experiment: high-altitude aircraft measurements in the tropical western Pacific. *Bull. Amer. Meteor. Soc.*, 98:129–144, 2017.

[21] A.R. Jones, D.J. Thomson, M. Hort, and B. Devenish. The U.K. Met Office's next-generation atmospheric dispersion model, NAME III. In Borrego C. and Norman A.-L., editors, *Air Pollution Modeling and its Application XVII, Proceedings of the 27th NATO/CCMS International Technical Meeting on Air Pollution Modelling and its Application*, pages 580–589. Springer, 2007.

[22] J.C. Lin, C. Gerbig, S.C. Wofsy, A.E. Andrews, B.C. Daube, K.J. Davis, and C. A. Grainger. A near-field tool for simulating the upstream influence of atmospheric observations: The Stochastic Time-Inverted Lagrangian Transport (STILT) model. *J. Geophys. Res.*, 108(D16):4493, 2003.

[23] R.H. Maryon, D.B. Ryall, and A.L. Malcolm. The NAME 4 dispersion model: Science documentation. Turbulence and Diffusion Note 262, Met Office, 1999.

[24] E. Meneguz and D.J. Thomson. Towards a new scheme for parametrization of deep convection in NAME III. *Int. J. Environ. Pollut.*, 54:128–136, 2014.

[25] M.A Navarro, E.L. Atlas, A. Saiz-Lopez, X. Rodriguez-Lloveras, D.E. Kinnison, J.-F. Lamarque, S. Tilmes, M. Filus, N.R.P. Harris, E. Meneguz, M.J. Ashfold, A.J. Manning, C.A. Cuevas, S.M. Schauffler, and V. Donets. Airborne measurements of organic bromine compounds in the Pacific tropical tropopause layer. *Proc. Natl. Acad. Sci. (USA)*, 112:13789–13793, 2015.

[26] L. L. Pan, E. L. Atlas, R. J. Salawitch, S. B. Honomichl, J. F. Bresch, W. J. Randel, E. C. Apel, R. S. Hornbrook, A. J. Weinheimer, D. C. Anderson, S. J. Andrews, S. Baidar, S. P. Beaton, T. L.

Campos, L. J. Carpenter, D. Chen, B. Dix, V. Donets, S. R. Hall, T. F. Hanisco, C. R. Homeyer, L. G. Huey, J. B. Jensen, L. Kaser, D. E. Kinnison, T. K. Koenig, J.-F. Lamarque, C. Liu, J. Luo, Z. J. Luo, D. D. Montzka, J. M. Nicely, R. B. Pierce, D. D. Riemer, T. Robinson, P. Romashkin, A. Saiz-Lopez, S. Schauffler, O. Shieh, M. H. Stell, K. Ullmann, G. Vaughan, R. Volkamer, and G. Wolfe. The convective transport of active species in the tropics (CONTRAST) experiment. *Bull. Amer. Meteor. Soc.*, 98:106–128, 2017.

[27] J. Petch, A. Hill, L. Davies, A. Fridlind, C. Jakob, Y. Lin, S. Xie, and P. Zhu. Evaluation of intercomparisons of four different types of model simulating TWP-ICE. *Quart. J. Roy. Meteor. Soc.*, 140:826–837, 2014.

[28] W.J. Randel and E.J. Jensen. Physical processes in the tropical tropopause layer and their roles in a changing climate. *Nature Geos.*, 6:169–176, 2013.

[29] A. Saiz-Lopez, J.M.C. Plane, A.R. Baker, L.J. Carpenter, R. von Glasow, J.C. Gmez Martn, G. McFiggans, and R.W. Saunders. Atmospheric chemistry of Iodine. *Chem. Rev.*, 112:1173–1804, 2012.

[30] A.F. Stein, R.R.Draxler, G.D. Rolph, B.J.B. Stunder, M.D. Cohen, and F. Ngan. NOAA's HYSPLIT atmospheric transport and dispersion modeling system. *Bull. Amer. Meteor. Soc.*, 96:2059–2077, 2015.

[31] A. Stohl, P. Seibert, G. Wotawa, D. Arnold, J.F. Burkhart, S. Eckhardt, and T.J. Yasunari. Technical note: the Lagrangian particle dispersion model FLEXPART version 6.2. *Atmos. Chem. Phys.*, 5:2461–2474, 2005.

[32] R.A. Stratton and A.J. Stirling. Improving the diurnal cycle of convection in GCMs. *Quart. J. Roy. Meteor. Soc.*, 138:1121–1134, 2012.

[33] D.J. Thomson. Criteria for the selection of stochastic models of particle trajectories in turbulent flows. *J. Fluid Mech.*, 180:529–556, 1987.

[34] D.J. Thomson and J.D. Wilson. History of Lagrangian stochastic models for turbulent dispersion. In Lin, Brunner, Gerbig, Stohl, Luhar, and Webley, editors, *Lagrangian Modeling of the Atmosphere*, pages 19–36. American Geophysical Union, 2013.

[35] M.C. vanZanten, B. Stevens, L. Nuijens, A.P. Siebesma, A.S. Ackerman, F. Burnet, A. Cheng, F. Couvreux, H. Jiang, M. Khairoutdinov, Y. Kogan, D. C. Lewellen, D. Mechem, K. Nakamura, A. Noda, B. J. Shipway, J. Slawinska, S. Wang, and A. Wyszogrodzki. Controls on precipitation and cloudiness in simulations of trade-wind cumulus as observed during RICO. *J. Adv. Model. Earth Syst.*, 3:M06001, 2011.

[36] D. Walters, A.J. Baran, I. Boutle, M. Brooks, P. Earnshaw, J. Edwards, K. Furtado, P. Hill, A. Lock, J. Manners, C. Morcrette, J. Mulcahy, C. Sanchez, C. Smith, R. Stratton, W. Tennant, L. Tomassini, K. Van Weverberg, S. Vosper, M. Willett, J. Browse, A. Bushell, K. Carslaw,

M. Dalvi, R. Essery, N. Gedney, S. Hardiman, B. Johnson, C. Johnson, A. Jones, C. Jones, G. Mann, S. Milton, H. Rumbold, A. Sellar, M. Ujiie, M. Whitall, K. Williams, and M. Zerroukat. The Met Office Unified Model Global Atmosphere 7.0/7.1 and JULES Global Land 7.0 configurations. *Geosci. Model Dev.*, 12:1909–1963, 2019.

Met Office
FitzRoy Road, Exeter
Devon, EX1 3PB
UK

Tel: 0370 900 0100
Fax: 0370 900 5050
enquiries@metoffice.gov.uk
www.metoffice.gov.uk

Produced with the Met Office LaTeX template v2.0.0